Journal of Nuclear Medicine, published on February 22, 2019 as doi:10.2967/jnumed.118.224170

Early phase I study of a ^{99m}Tc labeled anti-PD-L1 single domain antibody in SPECT/CT assessment of programmed death ligand-1 expression in non-small cell lung cancer

Yan Xing[§1], Gitasha Chand[§1,2], Changchun Liu[1], Gary J. R. Cook[3], Jim O'Doherty[4,5] Lingzhou Zhao[1], Nicholas C. L. Wong[2], Levente K. Meszaros[2], Hong Hoi Ting[2]* and Jinhua Zhao[1]*

[1] Department of Nuclear Medicine, Shanghai General Hospital, Shanghai Jiaotong University School of Medicine, People's Republic of China

[2] Nanomab Technology Limited, Shanghai, People's Republic of China

[3] Department of Cancer Imaging, School of Biomedical Engineering and Imaging Sciences, King's College London, London, United Kingdom

[4] Department of Molecular Imaging, Sidra Medicine, Doha, Qatar

[5] Weill Cornell Medical College, Education City, Doha, Qatar

---

* Corresponding authors: hhting@nano-mab.com (H. Ting) and zhaojinhua1963@126.com (J. Zhao)

[§] These authors equally contributed to this work.

First Authors: Gitasha Chand, 100 Haining Road, Shanghai. Phone: 86-13524200084, Email: gitashachand@nano-mab.com (not in training); Yan Xing, 100 Haining Road, Shanghai. Phone: 86-21-36126496, Email: xy.1@163.com (not in training).

For correspondence or reprints contact: Hong Hoi Ting. Nanomab Technology Limited. 2418 South Tower, 228 Weihai Road, Shanghai 200041.

Running Title: ^{99m}Tc-NM-01 SPECT/CT IMAGING OF PD-L1 Word Count: 4992

ABSTRACT

Purpose: Immunotherapy with checkpoint inhibitor programmed cell death 1 (PD-1)/programmed death ligand (PD-L1) antibodies demonstrates improvements in treatment of advanced non-small cell lung cancer (NSCLC). Treatment stratification depends on immunohistochemical PD-L1 measurement of biopsy material, an invasive method that does not account for spatiotemporal heterogeneity. Using a single domain antibody (sdAb), NM-01, against PD-L1, radiolabeled site-specifically with technetium-99m (^{99m}Tc) for single photon emission computed tomography (SPECT) imaging, we aimed to assess the safety, radiation dosimetry and imaging characteristics of this radiopharmaceutical and correlate tumor uptake with PD-L1 immunohistochemistry results. **Methods:** Sixteen patients (mean age 61.7 years, 11 male) with NSCLC were recruited. Primary tumor PD-L1 expression was measured by immunohistochemistry. NM-01 was radiolabeled with $[^{99m}Tc(OH_2)_3(CO)_3]^+$ complex binding to its C-terminal hexahistidine tag. Administered activity was 3.8-10.4 MBq/kg, corresponding to 100 μg or 400 μg of NM-01. Whole body planar and thoracic SPECT/CT scans were performed at 1 and 2h post-injection in all patients and 5 patients had additional imaging at 10mins, 3 and 24h for radiation dosimetry calculations. All patients were monitored for adverse events. **Results:** No drug-related adverse events occurred in this study. The mean effective dose was $8.84\times10^{-3} \pm 9.33\times10^{-4}$ mSv/MBq (3.59 ± 0.74 mSv per patient). Tracer uptake was observed in the kidneys, spleen, liver and bone marrow.

SPECT primary tumor-blood pool ratios (T:BP) varied from 1.24 to 2.3 (mean=1.79) at 1h and 1.24 to 3.53 (mean=2.22) at 2h (p=0.005). 2h primary T:BP ratios correlated with PD-L1 immunohistochemistry results (r=0.68, p=0.014). 2h T:BP was lower in tumors with ≤1% PD-L1 expression (1.89 vs 2.49, p=0.048). Nodal and bone metastases showed tracer uptake. Heterogeneity (>20%) between primary tumor and nodal T:BP was present in 4 of 12 patients. **Conclusion:** This first in human study demonstrates that ^{99m}Tc-labeled anti-PD-L1-sdAb SPECT/CT imaging is safe and associated with acceptable dosimetry. Tumor uptake is readily visible against background tissues, particularly at 2h when the T:BP ratio correlates with PD-L1 immunohistochemistry results.

Key Words: PD-L1; non-small cell lung cancer; SPECT/CT; Early Phase I; Single domain antibody (sdAb)

INTRODUCTION

Non-small cell lung cancer (NSCLC) is the leading cause of cancer mortality with nearly 1.6 million cancer related deaths p.a. worldwide *(1)*. Between 70-80% of patients present with unresectable advanced NSCLC at diagnosis and despite the development of molecular targeted therapies the prognosis of patients with advanced disease remains poor with an overall five-year survival rate of 15% (*2,3*). The recent breakthrough of immunotherapies with checkpoint inhibitor programmed cell death 1 (PD-1)/programmed death ligand (PD-L1) antibodies has demonstrated improvements in efficacy and tolerability over platinum-based chemotherapy in this subset of patients *(4-11)*. Six different PD-1/PD-L1 inhibitors have now been approved by the United States Food and Drug Administration for advanced NSCLC therapy.

PD-1 receptor, expressed on the surface of activated T-cells, is a negative co-stimulatory receptor and its ligands, PD-L1 or PD-L2, are normally expressed on the surface of dendritic cells or macrophages *(12,13)*. Certain malignancies have developed the ability to co-opt these immune checkpoints and escape the T-cell induced antitumor activity by overexpressing PD-L1 *(14,15)*.

Discrepancies in treatment response have highlighted potential deficiencies in the current methods to evaluate PD-L1 expression in a clinical setting *(16)*. Immunohistochemical assessment of tumor samples obtained by core needle biopsy is often unable to capture the heterogeneity and dynamic nature of PD-L1 expression within

the tumor and its microenvironment *(17).* In addition, core needle biopsy is not always practical (e.g. in patients with widespread metastatic or skeletal involvement) or may be of too high risk to be performed (e.g. certain mediastinal metastases). With the advent of immunotherapies, there is a need to develop a non-invasive imaging strategy to evaluate PD-L1 expression for optimal treatment stratification and monitoring.

Single domain antibodies (sdAbs) are the smallest naturally derived antigen-binding fragments from camelid antibodies and demonstrate great potential for molecular imaging in both preclinical and clinical models *(18-21).* Due to their low molecular weight (ca. 15 kDa) sdAbs rapidly clear from the circulation via the kidneys while retaining high target-binding potential. We developed a library of hexahistidine tagged anti-PD-L1 sdAbs that specifically bind to human PD-L1 without blocking PD-1/PD-L1 interaction. Due to them being designed to bind to a different domain of PD-L1, anti-PD-L1 immunotherapeutics will be unlikely to interfere with the binding of anti-PD-L1 sdAbs to PD-L1, thereby potentially allowing close monitoring of anti-PD-L1 immunotherapy by imaging. Recent studies demonstrated the potential of sdAbs for nuclear medicine imaging *(22)* .

Our hypothesis was that single photon emission computed tomography (SPECT) imaging of NSCLC with a ^{99m}Tc-labeled sdAb (^{99m}Tc-NM-01) that specifically binds to human PD-L1 is feasible, safe and correlates with PD-L1 immunohistochemistry results. In this first in human study we aimed to assess safety, radiation dosimetry and imaging

characteristics of ^{99m}Tc-NM-01 and sought to compare imaging and PD-L1 immunohistochemistry results in patients with advanced NSCLC.

MATERIALS AND METHODS

This was an open-label, non-randomized early phase I diagnostic study in patients with untreated NSCLC (n = 16) between March and November 2018 (ClinicalTrials.gov identifier no. NCT02978196) and obtained approval from Shanghai General Hospital Ethics Committee (Approval Number: 2016KY220). All patients enrolled into this study gave written informed consent in order to participate.

All materials used in the synthesis of ^{99m}Tc-NM-01 were prepared to good manufacturing practice standards. For details of anti-PD-L1 sdAb production, radiolabeling and quality control refer to Supplemental Materials. Briefly, to radiolabel NM-01 the $[^{99m}Tc(OH_2)_3(CO)_3]^+$ complex (pH 7.0-7.5) was added to a sealed vial containing 200 μg NM-01 in 100 μl phosphate buffered saline (pH 7.4) and the mixture was incubated at 37°C for 1 hour (*23-25*). Contents were diluted in physiological saline; in patient group 2 (see below), to adjust the injected dose to 400 μg per patient, additional NM-01 was added in this step.

Patients aged between 18 and 75 years with histopathologically confirmed NSCLC and Eastern Cooperative Oncology Group Performance Score (ECOG) of ≤1 were eligible to participate in this study (Supplemental Fig. 1). PD-L1 expression was

determined in primary tumor tissue obtained by core needle biopsy. Details of immunohistochemistry sample preparation and processing are reported in Supplemental Materials.

Patients received a single intravenous injection of ^{99m}Tc-NM-01 (3.8-10.4 MBq/kg), corresponding to 100 μg (group 1, n=13, 1.7 ± 0.3 μg/kg, range 1.2-2.1 μg/kg) or 400 μg (group 2, n=3, 5.9 ± 0.3 μg/kg, range 5.6-6.1 μg/kg), of NM-01. Whole body planar and thoracic tomographic imaging was performed on a GE Discovery NM07 SPECT/CT scanner (GE Healthcare, China) 1h and 2h after injection in all patients. One patient with known skeletal metastases had additional SPECT/CT acquisitions to include these sites. Adverse events were observed by monitoring vital signs, physical examination and clinical laboratory tests for each patient during a follow-up period of 7 days. Details of scanning protocol and monitoring of adverse events are reported in Supplemental Materials.

All scans were assessed by a single observer (GJRC) with over 25 years of nuclear medicine and radiology experience. Maximum counts were recorded from regions of interest (ROIs) drawn manually on SPECT scans, using the CT for guidance, around the primary tumor, any lymph node metastases within the thoracic field of view, a 3cm normal lung ROI in the right upper lobe (or left upper lobe if pathology existed in the right upper lobe) for tumor to lung ratios (T:L) and a ROI, within the aortic arch avoiding the walls of the aorta, for calculation of tumor to blood pool ratios (T:BP).

Radiation Dosimetry Calculations

Five patients underwent additional whole body planar imaging at 10min, 3h and 24h post-injection, to obtain radiation dosimetry data. No corrections were made for attenuation within the patient. A calibration source of 37 MBq at injection time was placed above the head of each patient to provide quantitative calibration of counts to activity. Radiation dosimetry calculations were performed by an experienced operator (JOD) in OLINDA/EXM dose calculation software (version 1.1) using well-known models (26,27). Imaging protocol and radiation dosimetry calculations are reported in Supplemental Materials.

Statistics

Differences and correlations between parameters were tested using the Wilcoxon signed rank test, Mann-Witney U-test and Spearman's correlation using IBM SPSS Statistics Version 24 software. A p value of <0.05 was taken for statistical significance.

RESULTS

Average radiochemical purity (RCP) of radiolabeled NM-01 was 96.9 ± 0.9% (95.4% - 98.5%), purification after radiolabeling was not necessary (Supplemental Fig. 2). Endotoxin levels remained below 0.4 EU/ml.

Patient Characteristics

16 patients (11 male, mean age 61.7 years) with histopathologically proven NSCLC (9 squamous cell carcinoma, 7 adenocarcinoma) were included. Clinical stage and other characteristics are summarized in Table 1. Uptake in lymph node metastases was observed in 12 patients. PD-L1 expression determined by immunohistochemistry ranged from 0 to 85% (Supplemental Fig. 3). The mean administered activity of ^{99m}Tc-NM-01 was 372 ± 62 MBq (range 255-485 MBq) in group 1 and 659 ± 25 MBq (range 635-685 MBq) in group 2 (Table 1).

Safety Assessment

^{99m}Tc-NM-01 was administered in 16 patients, no drug related adverse reactions were reported during the seven-day follow-up period. Symptoms related to advanced stage lung cancer, i.e. frequent coughing, dyspnea and fatigue, reported by some patients were not attributed to the radiopharmaceutical by the supervising physician (GC). Blood and urine clinical laboratory tests performed in the follow-up period were in the normal range of National Cancer Institute - Common Toxicology Criteria for Adverse Events version 4.0 standards. There were no significant changes recorded in clinical parameters such as heart rate, respiratory rate, body temperature and blood pressure during the follow-up. After participating in this study, patients proceeded with their treatment regimen.

Biodistribution

Tracer biodistribution in normal organs reflected physiological expression of PD-L1, with uptake observed in the lungs, liver, spleen and bone marrow (Fig. 1) (*28,29)*. Activity in these organs reduced with time and, in particular, lung and blood pool activity reduced between 1 and 2h in all patients allowing increased tumor to background conspicuity at 2h. Early diffuse lung activity that subsequently reduces may be as a result of a combination of blood pool and marginating immune cell activity (*30*). Renal activity persisting over 24h reflects excretion and possible renal tubular retention (Fig. 1).

No noticeable differences in image quality and no statistically significant differences in tumor to background ratio were observed between group 1 and group 2 (Fig. 1).

Radiation Dosimetry

Table 2 summarizes individual organ doses and effective doses for patients included in the dosimetry study (n=5). All patients had normal liver and kidney functions. The kidneys showed the highest organ dose (0.036 ± 0.018 mSv/MBq), followed by the bladder (0.026 ± 0.011 mSv/MBq), spleen (0.022 ± 0.011 mSv/MBq), and liver (0.011 ± 0.0025 mSv/MBq) and in line with the uptake and excretory pathway of the imaging agent. Time activity curves for organs with highest radiotracer uptake are shown in Figure 2.

Tumor activity and relationship with PD-L1 Immunohistochemistry

Primary tumor T:L ratio was greater at 2h than 1h (mean 2.69 vs 2.22, p=0.034) allowing reasonably good tumor conspicuity against normal background lung activity in

patients with high PD-L1 expression (Fig. 3; Table 3). Primary tumor T:BP ratio was also greater at 2h (mean 2.22 vs 1.79, p=0.005). Intratumoral heterogeneity of tracer uptake was noted in some primary tumors (Fig. 4). Patients with PD-L1 expression ≤ 1%, a level often used to stratify patients, showed significantly lower T:BP ratios (mean 1.89 vs 2.49, p=0.048). By receiver operating characteristic (ROC) analysis this gives an optimal threshold for 2h TBP of 2.32 (area under ROC = 0.88).

Thoracic lymph node metastases T:BP ratios were also greater at 2h although this difference did not reach statistical significance (mean 2.02 vs 1.83, p=0.12). At 2h, primary tumor and maximum lymph node metastasis T:BP ratios (n=12) showed a correlation (r=0.69, p=0.013). Intra-patient heterogeneity of T:BP ratios was noted between the primary tumor and lymph node metastases in several patients with a mean difference of 19% (± 17%), with 4 out of the 12 patients with lymph node metastases showing a greater than 20% difference (Fig. 5). If a 2h T:BP of 2.32 is used as a threshold for positivity, then only 3 out of the 13 patients with nodal disease would have been PD-L1 positive on SPECT. One patient with known bone metastases showed ^{99m}Tc-NM-01 uptake (Fig. 6). Primary tumor T:BP ratios at 2h correlated with PD-L1 immunohistochemistry results (r=0.68, p=0.014). Statistically significant correlations were not found for T:L ratios or 1h T:BP ratios.

DISCUSSION

This early phase 1 study demonstrates that ^{99m}Tc-NM-01 SPECT/CT imaging is a safe procedure, with no adverse events due to the radiopharmaceutical recorded in this cohort of patients. We achieved reproducibly high RCP in labeling NM-01. Radiation dosimetry is acceptable at $8.84\times10^{-3} \pm 9.33\times10^{-4}$ mSv/MBq (3.59 ± 0.74 mSv per patient) and similar to other SPECT agents in clinical use. The kidneys received the highest organ dose (0.036 ± 0.018 mSv/MBq) being the major route of excretion and although it remained tolerable, urinary tract dose could be further minimized by good hydration or co-injection of amino-acids or peptides (*31*).

Patients were administered either 100 µg or 400 µg of protein to explore specific binding in the liver and spleen, but no significant impact was observed in image quality or organ biodistribution. No statistically significant differences were noted in tumor to background ratios between the groups, therefore, subsequent studies were performed with 100 µg.

Biodistribution was as expected with early activity in the liver, spleen and kidneys and some activity in the lungs and bone marrow *(28)*. Rapid renal excretion allowed reduction of non-specific background blood pool and organ activity and enabled imaging at relatively early time points. In particular, rapid reduction in normal lung and blood pool activity allowed sufficient conspicuity of primary NSCLC and metastases on SPECT imaging. Imaging characteristics were more favorable at 2h post-injection compared to 1h due to reduction in lung and blood pool activity over this time.

Measurement of PD-L1 expression by immunohistochemistry is currently the method patients are stratified with for anti-PD-1/PD-L1 immunotherapy. Due to the heterogeneity of PD-L1 expression in lung cancers, biopsy material from one region of a tumor may not allow global or other regional assessment of PD-L1 expression *(32).* The underestimation of PD-L1 expression by sampling error in heterogenous tumors may be one of the reasons that apparent PD-L1 negative tumors respond to PD-1/PD-L1 checkpoint inhibitor therapy (*33-35*). Immunohistochemical evaluation is also limited by practicality and safety of multiple biopsies in patients with metastatic disease. Relying on immunohistochemistry results from tissue biopsy also limits the practicality of observing the evolution of PD-L1 expression in primary and metastatic tumors during therapy. For these reasons, a non-invasive imaging method that is safe and associated with low radiation dose, that can accurately report locoregional PD-L1 expression in primary tumors and metastases at serial time points, would be a valuable tool for guiding clinical management of patients with PD-L1 positive malignancies.

The use of ^{99m}Tc with a half-life of 6 hours and a straightforward site-specific labeling technique for NM-01 would allow distribution from centralized radiopharmacies as well as on-site labeling at any standard hospital radiopharmacy enabling widespread use of this methodology. There would also be future potential for labeling with PET radionuclides to help improve image spatial resolution, contrast and quantification *(32).*

Our intial results show promise that the simple measurement of T:BP ratios at 2h correlates with PD-L1 expression and if confirmed in subsequent studies could potentially replace or complement immunohistochemistry in some circumstances. We noted heterogeneity of activity within primary tumors in some patients, and between the primary tumor and metastases within patients, suggesting that intra- and inter-tumoral heterogeneity of PD-L1 expression is relatively common and is another factor that could be measured non-invasively with imaging to allow more relevant information to be available for patient treatment decisions. Intra-tumoral PD-L1 expression heterogeneity may also explain the imperfect correlation with T:BP (r=0.68).

A potential limitation of this study is the relatively small number of patients that were included, although it is similar to other phase 1 studies of radiopharmaceuticals and has sufficient power to allow statistical comparisons of optimal imaging time, radiodosimetry calculations and correlations with immunohistochemistry results. Immunohistochemical analysis was not available in all patients and only primary tumors were assessed therefore not allowing comparison between imaging and PD-L1 expression in nodal and distant metastases. SPECT images were acquired for up to 2 hours post-injection in all patients. To determine whether image characteristics (i.e. target-to-background) could be improved, further scanning beyond 2 hours could be considered in subsequent studies. The relatively low spatial resolution of SPECT does not allow more than gross visual intratumoral heterogeneity observations. Although a PET tracer, in

theory might allow more accurate and detailed heterogeneity analysis similar to what has been reported with ^{18}F-FDG PET/CT in NSCLC (*36*), recent studies with an anti-PD-L1 tracer for PET also reported on insufficient spatial resolution (*32*). In addition, we have only examined NSCLC in this study and cannot extrapolate these results to other malignancies that are known to express PD-1/PD-L1.

CONCLUSION

This study demonstrates that ^{99m}Tc labeled anti-PD-L1-sdAb SPECT/CT using ^{99m}Tc-NM-01 is a safe diagnostic procedure delivering a tolerable radiation dose, and presenting favorable biodistribution and image chacteristics correlating with PD-L1 immunohistochemistry results in patients with NSCLC. As PD-1/PD-L1 immune checkpoint inhibitors are more frequently used in the treatment of NSCLC, a companion imaging methodology is becoming increasingly sought-after for the staging and monitoring of patients. Anti-PD-L1-sdAb SPECT/CT using ^{99m}Tc-NM-01 has the potential to be used for the close monitoring of changes in PD-L1 expression levels during PD-L1 immunotherapy. In addition, the heterogeneous and dynamic nature of PD-L1 expression in most malignancies could make imaging a preferred method compared to more invasive core needle biopsies in diagnosing and staging patients with PD-L1 positive malignancies.

DISCLOSURE

This research is supported by Nanomab Technology Limited and Shanghai Shenkang Development Center for Clinical Skills Innovation (16CR3052A). The authors acknowledge financial support from the King's College London / University College London Comprehensive Cancer Imaging Centres funded by Cancer Research UK and Engineering and Physical Sciences Research Council in association with the Medical Research Council and the Department of Health (C1519/A16463) and the Wellcome Trust EPSRC Centre for Medical Engineering at King's College London (WT203148/Z/16/Z). No other potential conflict of interest relevant to this article exist.

ACKNOWLEDGMENTS

We would like to thank nuclear medicine technologist Ye Rong and nurses Qinli Qi and Ying Zhang for their assistance.

REFERENCES

1. Torre LA, Bray F, Siegel RL, Ferlay J, Lortet-Tieulent J, Jemal A. Global cancer statistics, 2012. *CA Cancer J Clin.* 2015;65:87-108.

2. Santini D, Barni S, Intagliata S, et al. Natural history of non-small cell lung cancer with bone metastases. *Sci Rep. 2015;5:18670.*

3. Besse B, Adjei A, Baas P, et al. 2nd ESMO Consensus Conference on lung cancer: non-small-cell lung cancer first-line/second and further lines of treatment in advanced disease. *Ann Oncol.* 2014;25:1475-84.

4. Fehrenbacher L, Spira A, Ballinger M, et al. Atezolizumab versus docetaxel for patients with previously treated non-small-cell lung cancer (POPLAR): a multicentre, open-label, phase 2 randomised controlled trial. *Lancet. 2016;387:1837-46.*

5. Rittmeyer A, Barlesi F, Waterkamp D, et al. Atezolizumab versus docetaxel in patients with previously treated non-small-cell lung cancer (OAK): a phase 3, open-label, multicentre randomised controlled trial. *Lancet.* 2017;389:255-265.

6. Zappa C, Mousa SA. Non-small cell lung cancer: current treatment and future advances. *Transl Lung Cancer Res*. 2016;5:288-300.

7. Masters GA, Temin S, Azzoli CG, et al. Systemic therapy for stage IV non-small cell lung cancer: American Society of Clinical Oncology Clinical Practice Guideline Update. *J Clin Oncol.* 2015;33:3488-515.

8. Garon EB, Rizvi NA, Hui R, et al. Pembrolizumab for the treatment of non–small-cell lung cancer. *New Engl J Med.* 2015;372:2018-2028.

9. Herbst RS, Baas P, Kim DW, et al. Pembrolizumab versus docetaxel for previously treated, PD-L1-positive, advanced non-small-cell lung cancer (KEYNOTE-010): a randomised controlled trial. *Lancet.* 2016;387:1540-1550.

10. Borghaei H, Paz-Ares L, Horn L, et al. Nivolumab versus Docetaxel in advanced nonsquamous non–small cell lung cancer. *New Engl J Med.* 2015;373:1627-1639.

11. Rizvi NA, Mazières J, Planchard D, et al. Activity and safety of nivolumab, an anti-PD-1 immune checkpoint inhibitor, for patients with advanced, refractory squamous

non-small-cell lung cancer (CheckMate 063): a phase 2, single-arm trial. *Lancet Oncol.* 2015;16:257-265.

12. Sharpe AH, Freeman GJ. The B7-CD28 superfamily. *Nat Rev Immunol.* 2002;2:116-26.

13. Keir ME, Butte MJ, Freeman GJ, Sharpe AH. PD-1 and its ligands in tolerance and immunity. *Annu Rev Immunol.* 2008;26:677-704.

14. Schreiber RD, Old LJ, Smyth MJ. Cancer immunoediting: integrating immunity's roles in cancer suppression and promotion. *Science.* 2011;331:1565-70.

15. Vesely MD, Kershaw MH, Schreiber RD, Smyth MJ. Natural innate and adaptive immunity to cancer. *Annu Rev Immunol.* 2011;29:235-71.

16. Kim ST, Klempner SJ, Park SH, et al. Correlating programmed death ligand 1 (PD-L1) expression, mismatch repair deficiency, and outcomes across tumor types: implications for immunotherapy. *Oncotarget.* 2017;8:77415-77423.

17. Ritprajak P, Azuma M. Intrinsic and extrinsic control of expression of the immunoregulatory molecule PD-L1 in epithelial cells and squamous cell carcinoma. *Oral Oncol.* 2015;51:221-8.

18. Vaneycken I, Devoogdt N, Van Gassen N, et al. Preclinical screening of anti-HER2 nanobodies for molecular imaging of breast cancer. *FASEB J.* 2011;25:2433-2446.

19. Xavier C, Vaneycken I, D'huyvetter M, et al. Synthesis, preclinical validation, dosimetry, and toxicity of 68Ga-NOTA-anti-HER2 Nanobodies for iPET imaging of HER2 receptor expression in cancer. *J Nucl Med.* 2013;54:776-784.

20. Keyaerts M, Xavier C, Heemskerk J, et al. Phase I study of 68Ga-HER2-nanobody for PET/CT assessment of HER2 expression in breast carcinoma. *J Nucl Med.* 2016;57:27-33.

21. Zhou Z, Vaidyanathan G, McDougald D, et al. Fluorine-18 labeling of the HER2-targeting single domain antibody 2Rs15d using a residualizing label and preclinical evaluation. *Mol Imaging Biol.* 2017;19:867-877.

22. Broos K, Lecocq Q, Raes G, Devoogdt N, Keyaerts M, Breckpot K. Noninvasive imaging of the PD-1: PD-L1 immune checkpoint: Embracing nuclear medicine for the benefit of personalized immunotherapy. *Theranostics.* 2018;8:3559.

23. Alberto R, Schibli R, Egli A, Schubiger AP, Abram U, Kaden TA. A novel organometallic aqua complex of technetium for the labeling of biomolecules: Synthesis of [99mTc(OH2)3(CO)3]+ from [99mTcO4]- in aqueous solution and its reaction with a bifunctional ligand. *J Am Chem Soc.* 1998;120:7987-7988.

24. Waibel R, Alberto R, Willuda J, et al. Stable one-step technetium-99m labeling of His-tagged recombinant proteins with a novel Tc (I)–carbonyl complex. *Nat Biotechnol.* 1999;17:897.

25. Badar A, Williams J, de Rosales RT, et al. Optimising the radiolabelling properties of technetium tricarbonyl and His-tagged proteins. *Eur J Nucl Med Mol Imaging Res.* 2014;4:14.

26. Stabin MG, Sparks RB, Crowe E. OLINDA/EXM: the second-generation personal computer software for internal dose assessment in nuclear medicine. *J Nucl Med.* 2005;46:1023-1027.

27. Hindorf C, Glatting G, Chiesa C, Linden O, Flux G, Committee ED. EANM Dosimetry Committee guidelines for bone marrow and whole-body dosimetry. *Eur J Nucl Med Mol Imaging.* 2010;37:1238-1250.

28. Josefsson A, Nedrow JR, Park S, et al. Imaging, biodistribution, and dosimetry of radionuclide-labeled PD-L1 antibody in an immunocompetent mouse model of breast cancer. *Cancer Res.* 2016;76:472-479.

29. Nedrow JR, Josefsson A, Park S, Ranka S, Roy S, Sgouros G. Imaging of Programmed Cell Death Ligand 1: Impact of protein concentration on distribution of anti-PD-L1 SPECT agents in an immunocompetent murine model of melanoma. *J Nucl Med.* 2017;58:1560-1566.

30. Igarashi T, Teramoto K, Ishida M, Hanaoka J, Daigo Y. Scoring of PD-L1 expression intensity on pulmonary adenocarcinomas and the correlations with clinicopathological factors. *ESMO Open.* 2016;1:e000083.

31. Bodei L, Mueller-Brand J, Baum RP, et al. The joint IAEA, EANM, and SNMMI practical guidance on peptide receptor radionuclide therapy (PRRNT) in neuroendocrine tumours. *Eur J Nucl Med Mol Imaging.* 2013;40:800-816.

32. Niemeijer A, Leung D, Huisman M, et al. Whole body PD-1 and PD-L1 positron emission tomography in patients with non-small-cell lung cancer. *Nat Comm* . 2018;9:4664.

33. Shen X, Zhao B. Efficacy of PD-1 or PD-L1 inhibitors and PD-L1 expression status in cancer: meta-analysis. *BMJ.2018;*362:k3529.

34. Ilie M, Long-Mira E, Bence C, et al. Comparative study of the PD-L1 status between surgically resected specimens and matched biopsies of NSCLC patients reveal major discordances: a potential issue for anti-PD-L1 therapeutic strategies. . *Ann Oncol.* 2016;27:147–153.

35. McLaughlin J, Han G, Schalper KA, et al. Quantitative assessment of the heterogeneity of PD-L1 expression in non-small-cell lung cancer. *JAMA Oncol.* 2016;2:46–54.

36. Cook GJ, Yip C, Siddique M, et al. Are pretreatment 18F-FDG PET tumor textural features in non-small cell lung cancer associated with response and survival after chemoradiotherapy? *J Nucl Med.* 2013;54:19-26.

Figure Legends

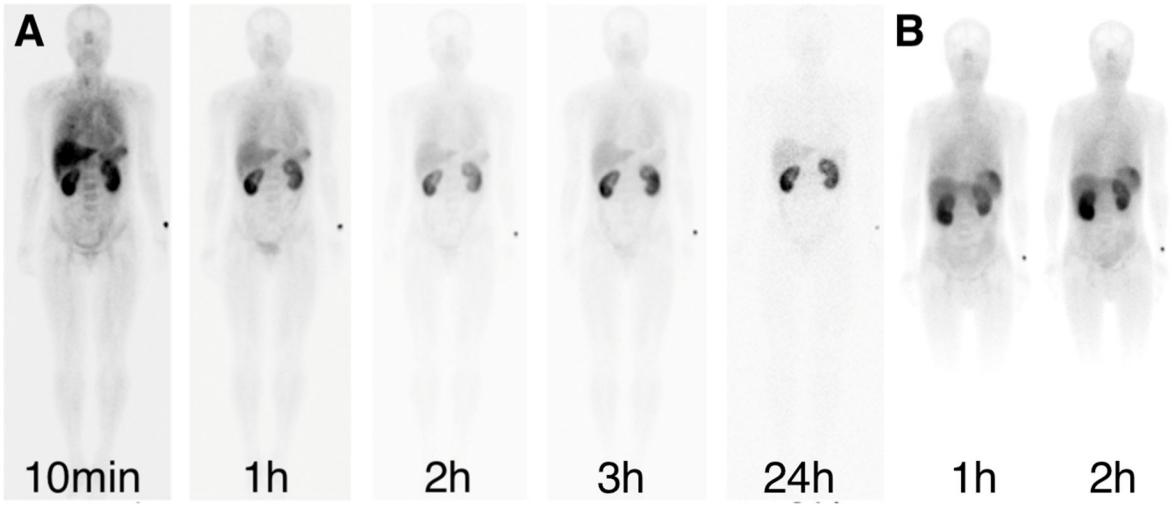

FIGURE 1. (A) anterior whole body images 10mins, 1, 2, 3 and 24hrs post-injection of a patient administered with 100 µg (group 1) and (B) 1 and 2h images of a patient administered with 400 µg of NM-01 (group 2). No significant difference in biodistribution was seen between the two groups.

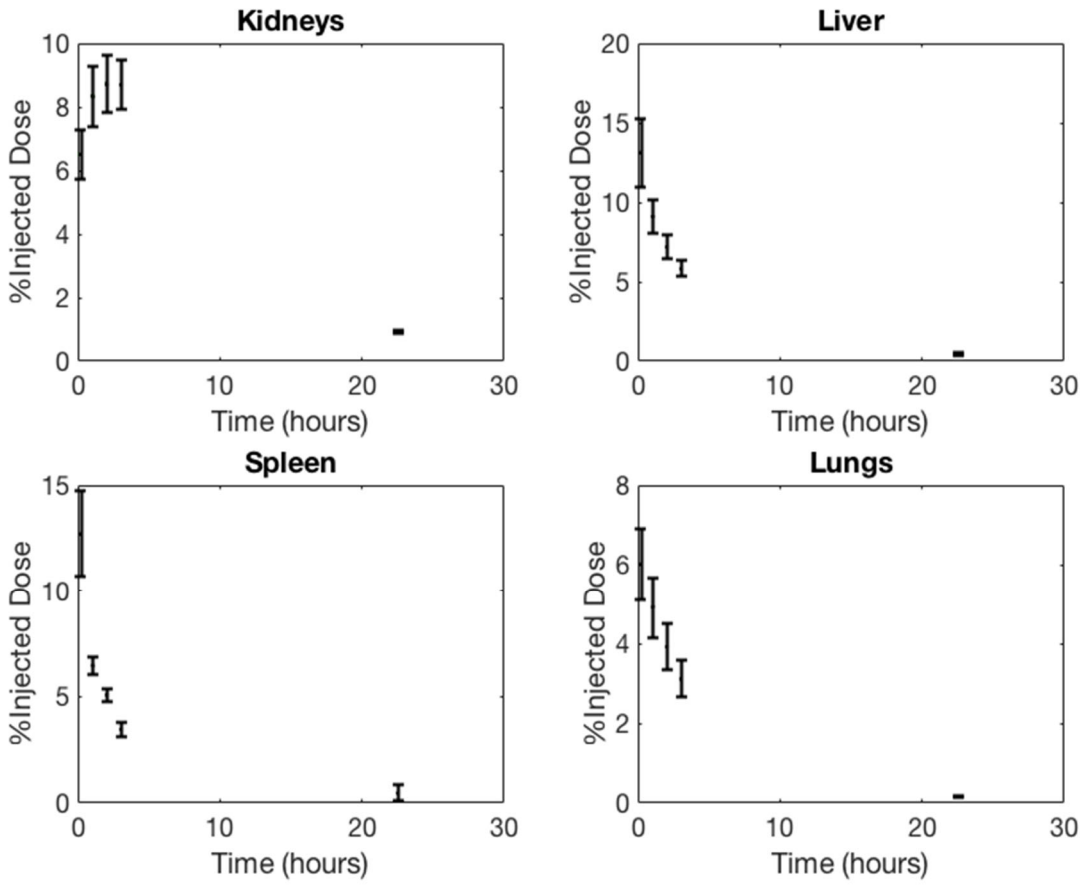

FIGURE 2. Time activity curves for organs with highest radiotracer uptake.

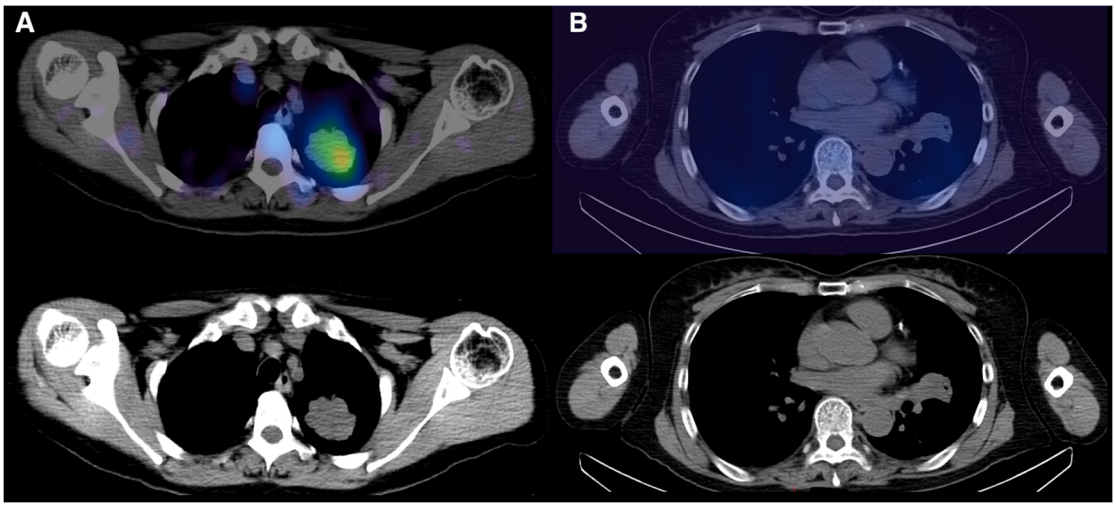

FIGURE 3. (A) Left upper lobe tumor T:BP = 3.12 (PD-L1 expression 50%), (B) left upper lobe tumor T:BP = 2.26 (PD-L1 expression 0%).

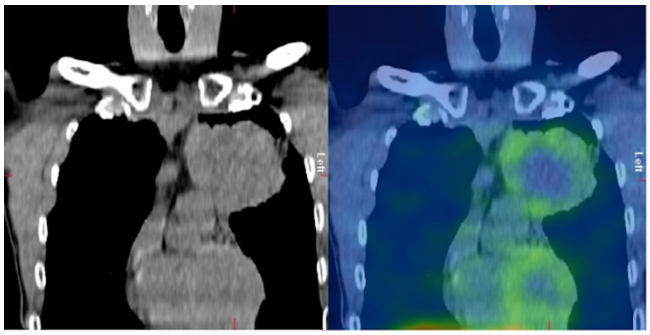

FIGURE 4. A left upper lobe tumor showing heterogeneity of PD-L1 expression. Central photopoenia is in keeping with necrosis but there is heterogeneity of uptake in the solid peripheral component of the tumor (T:BP = 2.46, PD-L1 expression 85%).

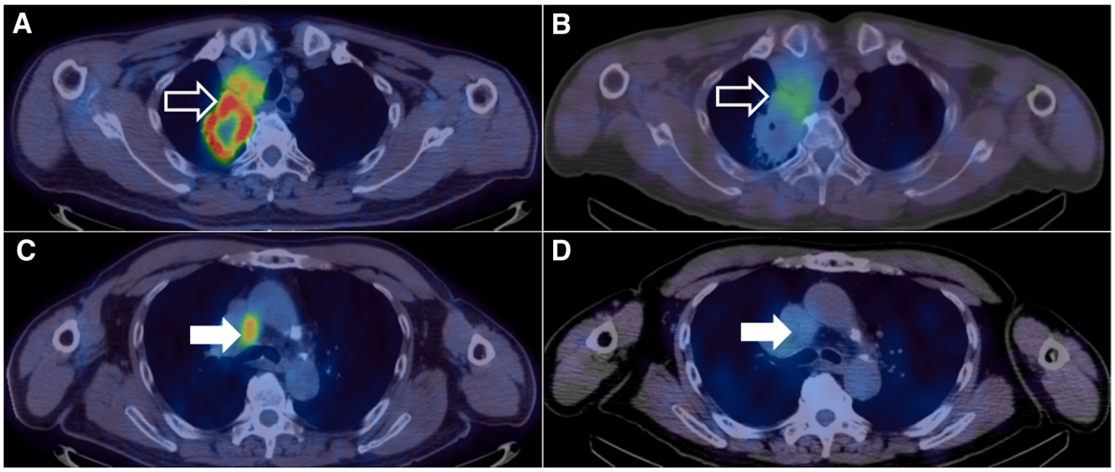

FIGURE 5. A right upper lobe tumor (open arrows) shows areas of high FDG uptake (SUVmax = 16.1) on PET/CT (A) and ^{99m}Tc-SPECT/CT (T:BP = 3.53) (B) Mediastinal lymph nodes (closed arrows) show high FDG uptake (SUVmax = 6.3) (C) but low ^{99m}Tc-NM-01 activity (T:BP = 1.13) (D) demonstrating heterogeneity of PD-L1 expression between primary tumor and nodal sites of disease within the same patient.

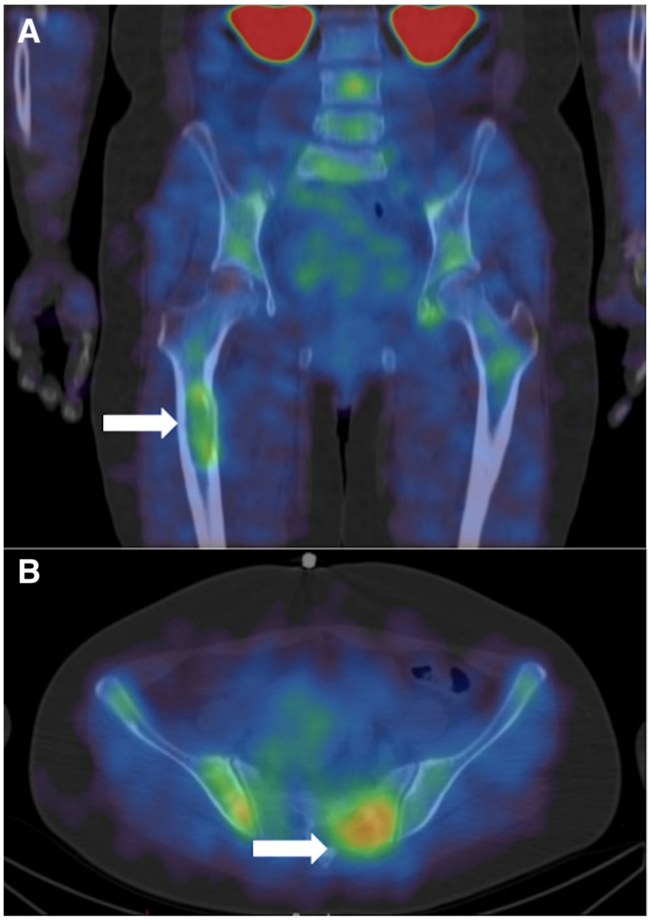

FIGURE 6. Coronal (A) and axial (B) ^{99m}Tc-NM-01 SPECT/CT images of a patient with skeletal metastases (arrows) demonstrating PD-L1 expression.

Tables

Table 1: Patient Characteristics

Dose Group	Patient No.	Age	Gender	Tumor Type	Tumor Size (CT axial dimensions)	Clinical Staging	PD-L1 Expression (%)	ECOG Score
Group 1 3.8-8.4 MBq/kg- 1.2-2.1 µg/kg	1	49	Male	Adenocarcinoma	37*27mm	cT4N3M1 IV	NA	1
	2	75	Male	Squamous Cell Carcinoma	44*48mm	T3N3M1 IV	20	1
	3	75	Male	Squamous Cell Carcinoma	55*46mm	T2bN3M0 IIIB	0	1
Group 2 9.1-10.4 MBq/kg- 5.6-6.1 µg/kg	4	65	Male	Adenocarcinoma	48*42 mm	T2bN3M1 IV	0	0
	5	57	Male	Squamous Cell Carcinoma	32*35 mm	cT2N2M0 IIIA	55	0
	6	65	Male	Squamous Cell Carcinoma	30*58 mm	T2aN2M0 IIIA	3	0
Group 1 3.8-8.4 MBq/kg- 1.2-2.1 µg/kg	7	75	Female	Adenocarcinoma	38*28mm	T2aN0M0	NA	0
	8	52	Female	Squamous Cell Carcinoma	33*23mm	T2aN0M0 1B	0	0
	9	36	Female	Adenocarcinoma	45*35mm	T2aN2M1 IV	1	1
	10	46	Female	Adenocarcinoma	42*35mm	T3N1M0 IIIA	50	0
	11	51	Male	Squamous Cell Carcinoma	47*35mm	T2aN3M0 IIIB	2	0
	12	72	Male	Adenocarcinoma	46*53mm	T2bN3M1 IV	NA	1
	13	55	Male	Squamous Cell Carcinoma	71*78mm	T4N0M1c IV	85	0
	14	69	Male	Squamous Cell Carcinoma	20*28mm	T3N1M0 IIIA	10	0
	15	71	Female	Squamous Cell Carcinoma	78*95mm	T4N1M1a IV	NA	1
	16	60	Male	Adenocarcinoma	93*75mm	T4N3M1a IV	2	0

*NA= not available

Table 2: Organ Radiation Doses

Organ/tissue	Mean (mSv/MBq)	SD (mSv/MBq)
Adrenals	5.54E-03	1.80E-03
Brain	1.41E-03	4.15E-04
Breasts	1.66E-03	5.86E-04
Gallbladder	4.89E-03	1.69E-03
Lower large intestine wall	4.00E-03	9.79E-04
Small intestine	3.88E-03	1.13E-03
Stomach	6.04E-03	1.71E-03
Upper large intestine wall	3.72E-03	1.15E-03
Heart wall	3.17E-03	1.04E-03
Kidneys	3.60E-02	1.76E-02
Liver	1.10E-02	2.51E-03
Lungs	4.53E-03	1.23E-03
Muscle	2.62E-03	8.35E-04
Ovaries	4.11E-03	1.01E-03
Pancreas	5.72E-03	2.01E-03
Red Marrow	6.73E-03	3.25E-03
Osteogenic cells	8.08E-03	1.74E-03
Skin	1.49E-03	5.46E-04
Spleen	2.21E-02	1.14E-02
Testes	2.44E-03	8.40E-04
Thymus	2.32E-03	7.89E-04
Thyroid	4.00E-03	2.25E-02
Urinary Bladder wall	2.58E-02	1.05E-02
Total body	3.20E-03	9.13E-04
Effective Dose	**8.84E-03**	**9.33E-04**

Table 2: Radiation absorbed doses calculated by OLINDA/EXM software and overall effective dose (mSv/MBq) (n=5).

Table 3: Imaging characteristics

Patient no.	sdAb dose group	Injected activity (MBq)	SPECT T:L ratio 1h	SPECT T:L ratio 2h	SPECT T:BP ratio 1h	SPECT T:BP ratio 2h	SPECT highest lymph node T:BP ratio 1h	SPECT highest lymph node T:BP ratio 2h
1	1	339	1.92	2.17	1.31	1.24	1.84	1.64
2	1	374	2.82	2.99	2.03	3.09	1.99	3.40
3	1	375	2.16	2.80	1.25	1.65	1.31	1.73
4	2	656	1.19	1.44	1.24	1.66	1.43	1.73
5	2	685	0.93	1.10	2.23	2.65	1.65	1.95
6	2	635	2.71	1.88	1.75	1.79	2.22	3.24
7	1	255	1.80	2.06	1.31	1.76	NP	NP
8	1	398	2.48	2.41	1.83	2.26	NP	NP
9	1	486	1.42	2.07	1.95	2.00	2.1	1.9
10	1	381	3.15	5.63	2.13	3.12	1.47	1.75
11	1	317	1.92	1.74	1.73	2.37	1.39	2.26
12	1	448	4.17	6.50	2.20	3.53	3.05	3.13
13	1	400	2.4	3.09	1.61	2.46	NP	NP
14	1	409	1.49	1.54	1.68	1.98	1.75	1.34
15	1	289	1.69	1.47	2.16	1.55	1.9	1.77
16	1	363	3.35	4.15	2.3	2.47	2.23	2.09
Mean			2.22	2.69	1.79	2.22	1.83	2.02
Median			2.04	2.12*	1.79	2.13**	1.84	1.77^{+}

Table 3: T:L primary tumor to lung ratio, T:BP primary tumor to blood pool ratio,

*p=0.034 between 1 and 2h, **p=0.005 between 1 and 2h, +p=Not Significant; NP= not present

Supplemental Data

Safety Assessment

All patients underwent measurement of vital signs (blood pressure, respiratory rate, heart rate, and body temperature) during screening period (up to 7 days before scan), before injection and then every 60 minutes up to 5 hours post-injection and first follow up period (48h after SPECT/CT scan). Clinical laboratory testing, including standard hematologic and comprehensive metabolic panels i.e. total red blood cell count, total white blood cell count, neutrophil count, lymphocyte count, platelet count, plasma creatinine, plasma blood urea nitrogen, plasma ionized calcium, sodium, potassium, lactate dehydrogenase, alanine aminotransferase (ALT), aspartate aminotransferase (AST), alkaline phosphatase, total serum bilirubin and serum albumin) were performed during the screening period (no more than 14 days before scan) and the follow-up period (48h after SPECT/CT scan). In an additional step to ensure safety of patients, a phone interview was conducted 7 days after the SPECT/CT scan to follow up on patients, and a questionnaire was filled out by the investigator as presented in the Case Report Form (CRF). If no adverse reactions were reported by the patient during the phone interview, the patient's activities in this study were deemed to be completed. Patient recruitment, intervention allocation, follow up and analysis are described in Supplemental Figure 1.

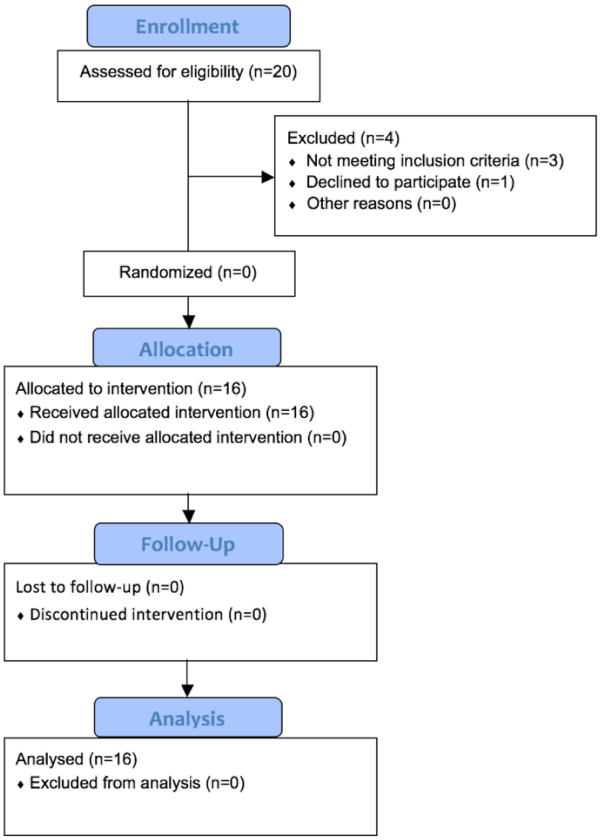

Supplemental Figure 1: CONSORT flowchart of patient enrollment, allocation, follow-up and analysis.

SPECT/CT Scan Protocol

Patients were administered ^{99m}Tc-NM-01 in an intravenous bolus (3.8-10.4 MBq/kg), corresponding to 100 µg (group 1, n=13, 1.7 ± 0.3 µg/kg, range 1.2-2.1 µg/kg) or 400 µg (group 2, n=3, 5.9 ± 0.3 µg/kg, range 5.6-6.1 µg/kg) of NM-01. Patients were asked to drink 300-500ml of water after injection then void their bladder before imaging on a GE Discovery NM07 SPECT/CT scanner (GE Healthcare, China). Planar scans were acquired in supine position at 1h and 2h after injection at 10cm/slice/min. CT scan was acquired at 60 min followed by local tomographic SPECT imaging focused around primary and suspected secondary as follows. All scans were acquired using low-energy high-resolution collimators in a 20% energy window

centered around 140 keV, in a 256 × 1024 matrix for planar images and 64 × 64 matrix for tomographic images. A 10% energy window centered around 120 keV was also collected during tomographic acquisitions for attenuation and scatter correction. SPECT images were acquired over 360° in 60 frames per full rotation with 20 seconds acquisition per frame.

Radiation Dosimetry Calculations

Five patients underwent extra whole body planar imaging at additional time points, i.e. 10min, 1h, 2h, 3h and 24h post-injection, to obtain radiation dosimetry data. A calibration source of 37 MBq at injection time was placed above the head of each patient in order to provide quantitative calibration of counts to activity. Visible organs were drawn on the initial anterior and posterior whole body images for each patient at 10 minutes using OsiriX software (Pixmeo, Switzerland) by an experienced operator (JOD) and transferred to all remaining timepoints. The remainder of body was assigned activity not accounted for by organ delineation or excretion. All organs for each patient were assumed to be of the same volume over the imaging timeframe. Counts from the anterior and posterior images were geometrically averaged. Time-activity curves were converted to % injected dose (%ID), and used as an input to the OLINDA/EXM dose calculation software (version 1.1) (*1*). Organ normalized cumulated activities (NCA) were automatically calculated using the net injected activity and organ volume of the male standard 70-kg Cristy–Eckerman adult anthropomorphic phantom used by OLINDA/EXM. Time–activity curves were fitted to biexponential functions where possible, assuming radionuclide decay (i.e. no further excretion) on reaching the last imaging point. Red bone marrow dosimetry was calculated from outlining of the lumbar vertebrae and using a well-known model whereby the lumbar vertebrae contain 12.3% of red bone marrow in adults (*2*). NCA of the urinary bladder contents was calculated using a dynamic

urinary bladder model in the OLINDA/EXM using a 3.5-h voiding interval as recommended by the International Commission on Radiological Protection.

NM-01 production and formulation

The anti-PD-L1 sdAb NM-01 was produced to good manufacturing practice (GMP). The sequence with carboxy terminal hexahistidine tail was subcloned in expression vector pE7 and produced in Escherichia coli BLR(DE3). The expressed sdAb was further purified from periplasmic extracts by cation exchange chromatography on SP Sepharose (GE Healthcare, USA) and buffer exchanged to phosphate buffered saline (PBS) with gel filtration on Superdex 75 resin (GE Healthcare, USA). sdAb concentration was adjusted to 2.0 mg/ml in PBS and 100 µl NM-01 aliquots, containing 200 µg NM-01 were aseptically dispensed into septum sealed sterile glass vials. Aliquots were stored at -80^{o}C until use.

Preparation of the $[^{99m}Tc(OH_2)_3(CO)_3]^+$ complex

All ingredients used in the preparation of $[^{99m}Tc(OH_2)_3(CO)_3]^+$ complex and subsequent radiolabeling of NM-01 were sterile and prepared to GMP standards. Sodium pertechnetate in physiological saline was obtained from a $^{99}Mo/^{99m}Tc$ generator. The $[^{99m}Tc(OH_2)_3(CO)_3]^+$ complex was prepared in solution using an in situ CO source (*3*). To a septum-sealed glass vial containing 4.5 mg $Na_2[H_3BCO_2]$, 2.85 mg $Na_2B_4O_7 \cdot 10H_2O$, 7.15 mg Na_2CO_3 and 8.5 mg $Na_2C_4H_4O_6 \cdot 2H_2O$ under argon 2146-4810 MBq sodium pertechnetate were added in 1.0 ml physiological saline. The vial was incubated in a boiling waterbath for 30 minutes. Following incubation, the vial was cooled to room temperature and 180 µl 1.0 M HCl were added to bring the pH to 7.0-7.5.

QC of the $[^{99m}Tc(OH_2)_3(CO)_3]^+$ complex was performed by thin layer chromatography (TLC) in a system consisting of silica gel 60 F254 TLC plates (Merck, Germany) and 1% HCl in methanol

mobile phase. In this TLC system colloidal ^{99m}Tc has a retention factor (R_f) of 0; $[^{99m}Tc(OH_2)_3(CO)_3]^+$ is represented by a broad peak with an average R_f=0.4-0.5 and $^{99m}TcO_4^-$ has an R_f=1. Only $[^{99m}Tc(OH_2)_3(CO)_3]^+$ with a radiochemical purity (RCP) >95% was used for NM-01 radiolabeling. In this step RCP was defined as ^{99m}Tc radioactivity associated with $[^{99m}Tc(OH_2)_3(CO)_3]^+$ as a percentage of total ^{99m}Tc radioactivity on the plate.

Radiolabeling NM-01 and preparation of patient doses

To a 200 µg aliquot of NM-01 in 100 µl sterile PBS 400 µl $[^{99m}Tc(OH_2)_3(CO)_3]^+$ pH 7.0-7.5, corresponding to 670-1510 MBq were added. The vial was incubated at 37°C for 1 hour. In group 1, 1.5 ml saline were added to the kit vial containing ^{99m}Tc-NM-01 after incubation, bringing the total volume to 2.0 ml. In group 2, in place of 1.5 ml saline 500 µg NM-01 in 1.25 ml saline were added to the kit vial after incubation, bringing the total volume to 1.75 ml. QC tests, including visual check and assessment of RCP, pH measurement and evaluation of endotoxin levels were performed. RCP testing was routinely performed by TLC in a system consisting of silica gel coated instant thin layer chromatography (ITLC-SG) plates (Agilent Technologies, USA) and citrate buffer pH 5.4 mobile phase. In this system ^{99m}Tc radiolabeled NM-01 has R_f=0 and unreacted $[^{99m}Tc(OH_2)_3(CO)_3]^+$ and $^{99m}TcO_4^-$ both have R_f=1. ^{99m}Tc-NM-01 with RCP>95%, pH=7.0-7.5, endotoxin levels <15 EU/ml with a colorless, clear appearance was deemed acceptable for use in this study. RCP in this step was defined as ^{99m}Tc radioactivity associated with NM-01 as a percentage of total ^{99m}Tc radioactivity on the plate. Since RCP exceeded 95% in every case purification after radiolabeling was not necessary. For patient injection 1.0 ml of the final solution, corresponding to 286 – 546 MBq/100 µg ^{99m}Tc-NM-01 (group 1) or 697 - 736 MBq/400 µg ^{99m}Tc-NM-01 was withdrawn aseptically into a 2.0 ml syringe.

High performance liquid chromatography (HPLC) characterization of ^{99m}Tc-NM-01

The radiolabeled NM-01 was characterized by size exclusion (SEC) chromatography. SEC HPLC analyses were performed in an Agilent 1200 HPLC system (Agilent Technologies, USA) consisting of a manual injector and quaternary solvent pump, coupled to a Phenomenex BioSep SEC-s2000, 5 μm, 145A, 300x7.8 mm column fitted with a Phenomenex Securityguard GFC2000 4x3 mm guard cartridge (both Phenomenex, USA), connected to a single channel variable wavelength detector (Agilent Technologies, USA) and a BioScan Flowcount gamma detection unit (BioScan, USA). Analyses were performed in isocratic 45% acetonitrile – 0.1% trifluoroacetic acid in water at a flow rate of 1 ml/min over 30 minutes with UV detection at 280 nm. In this system the ^{99m}Tc-NM-01 is represented by a single peak at 6min 47 sec ± 2 sec (n=4), the $[^{99m}Tc(OH_2)_3(CO)_3]^+$ complex is represented by a single peak at 10min 40 sec ± 2 sec (n=3) and $^{99m}TcO_4^-$ is represented by a single peak at 21min 34 sec ± 20 sec (n=4). A representative HPLC radiochromatogram of ^{99m}Tc-NM-01 is presented in Supplemental Figure 2. Radiolabeling and quality control method development will be published elsewhere.

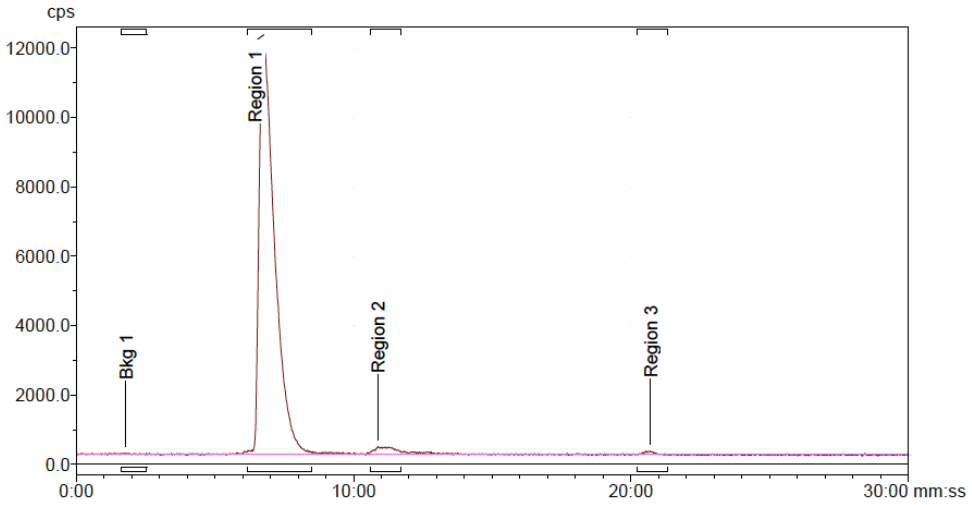

Supplemental Figure 2: HPLC radiochromatogram of ^{99m}Tc-NM-01 (Region 1: ^{99m}Tc-NM-01 (6:47, 97.7%), Region 2: [^{99m}Tc$(OH_2)_3(CO)_3]^+$ (10:47, 2.0%), Region 3: $^{99m}TcO_4^-$ (20:52, 0.3%).

Immunohistochemical Methodology and Results

Primary tumor samples, 1-2 mm in diameter, were obtained by core needle biopsy for immunohistochemical evaluation of PD-L1 expression. Tissue slice controls included placental tissue as negative control and tonsil tissue as positive control, as well as confirmed positive and negative NSCLC tumor tissues. A control cell slide mounted with a PD-L1 positive and negative cell pellet (DAKO North America, USA) was also processed in parallel (images presented in Supplemental Figure 3). After collection, formalin-fixed paraffin-embedded (FFPE) blocks were prepared according to instructions set in the PD-L1 IHC 22C3 pharmDx immunohistochemical assay kit manual (DAKO North America, USA). Briefly, each specimen was fixed in 10% neutral buffered formalin. After rinsing, samples were dehydrated by sequential immersion in ascending concentrations of ethanol in water for 2 hours at each concentration; starting at 80% and reaching

100% in 5% increments. Dehydrated samples were cleared in xylene and subsequently infiltrated with melted paraffin at 55°C.

FFPE blocks were cut into 4 μm sections in a Leica RM2235 Rotary Microtome (Leica Biosystems, Germany). Sections were mounted onto DAKO Flex IHC microscope slides (DAKO North America, USA), stored in the dark at 2-8°C and used within 30 days of preparation.

Further processing and immunostaining of primary tumor samples and controls were performed in a DAKO Autostainer Link 48 SK006 immunohistochemistry stainer (DAKO North America, USA) using the pre-programmed 'PD-L1 IHC 22C3 pharmDx' staining protocol and reagents, including the mouse anti-PD-L1 (clone 22C3), provided in the assay kit. Briefly, an automated three-in-one process of deparaffinisation, sample rehydration and target retrieval was followed by an automated staining procedure with mouse anti-PD-L1 (clone 22C3) antibody, followed by hematoxylin (Baso Diagnostic Inc., Taiwan) counterstaining. Microscopic and histopathological evaluation of PD-L1 immunostaining were performed on DAKO Autostainer Link 48 (DAKO North America, USA) and results validated by a pathologist. Representative images were recorded using a Leica DM6000B microscope (Leica Biosystems, Germany) and Leica DFC 550 digital camera (Leica Biosystems, Germany).

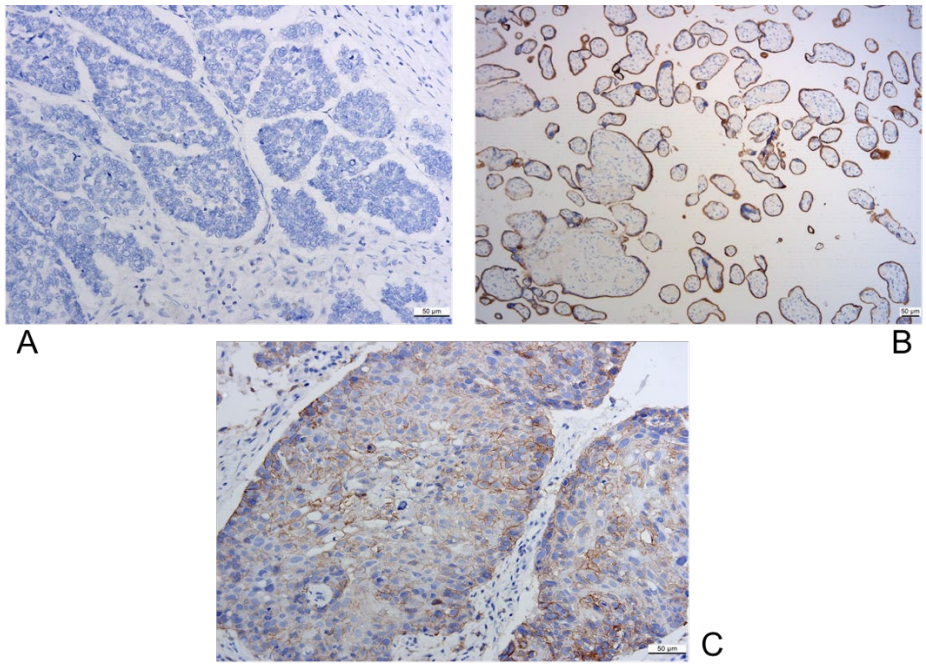

Supplemental Figure 3: PD-L1 immunohistochemical staining of (A) negative control, (B) positive control and (C) Patient 5 primary tumor tissue showing 55% expression.

References:

1. Stabin MG, Sparks RB, Crowe E. OLINDA/EXM: the second-generation personal computer software for internal dose assessment in nuclear medicine. *J Nucl Med.* 2005;46:1023-1027.

2. Hindorf C, Glatting G, Chiesa C, Linden O, Flux G, Committee ED. EANM Dosimetry Committee guidelines for bone marrow and whole-body dosimetry. *Eur J Nucl Med Mol Imaging.* 2010;37:1238-1250.

3. Alberto R, Schibli R, Egli A, Schubiger AP, Abram U, Kaden TA. A Novel Organometallic Aqua Complex of Technetium for the Labeling of Biomolecules: Synthesis of [99mTc(OH2)3(CO)3]+ from [99mTcO4]- in Aqueous Solution and Its Reaction with a Bifunctional Ligand. *Journal of the American Chemical Society.* 1998;120:7987-7988.